7-14-2010

Deconvolution of u channel magnetometer data: Experimental study of accuracy, resolution, and stability of different inversion methods

Mike J. Jackson
University of Minnesota - Twin Cities, jacks057@umn.edu

Julie A. Bowles
University of Wisconsin-Milwaukee, bowlesj@uwm.edu

Ioan Lascu

Peter A. Solheid
University of Minnesota - Twin Cities

Click Here for Full Article

Deconvolution of u channel magnetometer data: Experimental study of accuracy, resolution, and stability of different inversion methods

Mike Jackson, Julie A. Bowles, Ioan Lascu, and Peat Solheid

Institute for Rock Magnetism, Department of Geology and Geophysics, University of Minnesota, 291 Shepherd Laboratories, 100 Union Street SE, Minneapolis, Minnesota 44544, USA (irm@tc.umn.edu)

[1] We explore the effects of sampling density, signal/noise ratios, and position-dependent measurement errors on deconvolution calculations for u channel magnetometer data, using a combination of experimental and numerical approaches. Experiments involve a synthetic sample set made by setting hydraulic cement in a 30-cm u channel and slicing the hardened material into ~2-cm lengths, and a natural lake sediment u channel sample. The cement segments can be magnetized and measured individually, and reassembled for continuous u channel measurement and deconvolution; the lake sediment channel was first measured continuously and then sliced into discrete samples for individual measurement. Each continuous data set was deconvolved using the ABIC minimization code of Oda and Shibuya (1996) and two new approaches that we have developed, using singular-value decomposition and regularized least squares. These involve somewhat different methods to stabilize the inverse calculations and different criteria for identifying the optimum solution, but we find in all of our experiments that the three methods converge to essentially identical solutions. Repeat scans in several experiments show that measurement errors are not distributed with position-independent variance; errors in setting/determining the u channel position (standard deviation ~0.2 mm) translate in regions of strong gradients into measurement uncertainties much larger than those due to instrument noise and drift. When we incorporate these depth-dependent measurement uncertainties into the deconvolution calculations, the resulting models show decreased stability and accuracy compared to inversions assuming depth-independent measurement errors. The cement experiments involved varying directions and uniform intensities downcore, and very good accuracy was obtained using all of the methods when the signal/noise ratio was greater than a few hundred and the sampling interval no larger than half the length scale of magnetization changes. Addition of synthetic noise or reduction of sampling density decreased the resolution and accuracy of all the methods equally. The sediment-core experiment involved uniform (axial) magnetization direction and strongly varying intensities downcore. Intensity variations are well resolved and directions are accurate to within about 5 degrees, with errors attributable to omission and/or inaccurate calibration of cross terms in the instrument response function.

Theme: Advances in Instrumentation for Paleomagnetism and Rock Magnetism
Guest Editors: M. Fuller, B. Goodman, J. Kirschvink, and K. Verosub

---

1. Introduction

[2] Continuous sediment cores are among the most important sources of information on paleomagnetic field behavior, offering the possibility of high-resolution records of the changing field orientation and strength through time [*Tauxe et al.*, 1983; *Weeks et al.*, 1993; *Roberts*, 2006]. As is well known, however, the paleofield signal can be modified by filtering effects, both during the recording process (lock-in over an interval of depth and time [e.g., *Teanby and Gubbins*, 2000; *Roberts and Winklhofer*, 2004; *Liu et al.*, 2008; *Shcherbakov and Sycheva*, 2010]) and during measurement on long-core magnetometers with broad (~decimeter) sensitivity functions (i.e., convolution [*Dodson et al.*, 1974; *Constable and Parker*, 1991; *Oda and Shibuya*, 1996]). The filter function of the magnetometer can be determined from experimental data [e.g., *Parker and Gee*, 2002] or by numerical calculation [*Shibuya and Michikawa*, 2000], and its effects can be removed by deconvolution [*Dodson et al.*, 1974; *Constable and Parker*, 1991; *Weeks et al.*, 1993; *Oda and Shibuya*, 1996; *Guyodo et al.*, 2002].

[3] The accuracy and reliability of deconvolution calculations depend on the validity of several key assumptions, including: (a) that the measurement errors have a Gaussian distribution with zero mean, independent of measurement position; (b) that magnetization intensity and orientation vary only as a function of depth $\vec{M}(z)$; (c) that the variations in $\vec{M}(z)$ are reasonably smooth and that the smoothness of the magnetization is similar throughout the core and (d) that the instrument response function is accurately known. Relatively few published studies have directly tested the validity of magnetization models derived by deconvolution of continuous-core measurements [*Constable and Parker*, 1991; *Weeks et al.*, 1993; *Oda and Shibuya*, 1996; *Guyodo et al.*, 2002], and comparison with discrete-sample measurements has generally shown agreement ranging from fair to very good. *Oda and Shibuya* [1996] compared their deconvolved split-core record with discrete-sample data of *Schneider*

et al. [1992], and concluded that assumptions b and d above were not completely fulfilled in their study, constituting the largest sources of inaccuracy in their deconvolution results. *Guyodo et al.* [2002] cut 1-cm slices from a u channel after continuous measurements; the slices showed considerably more variability than the deconvolved u channel record, and they attributed the differences to possible disturbance and position errors during subsampling, or incomplete accuracy in their response function model. *Weeks et al.* [1993] measured a set of discrete $2 \times 2 \times 2$ cm cubes before assembling them into a "train" for measurement as a continuous core, which yielded a deconvolved magnetization distribution in quite good directional agreement with the discrete measurements, but somewhat less good agreement with regard to intensity.

[4] In this study we use experimental methods similar to those of *Weeks et al.* [1993] to evaluate several numerical approaches to deconvolution. We employ the ABIC-minimization code of *Oda and Shibuya* [1996], which was also used by *Guyodo et al.* [2002], and which remains the state of the art. This software treats the response function as a tensor [e.g., *Parker and Gee*, 2002], albeit incompletely; i.e., it accommodates the magnetometer x-sensor response to the x- and z-components of magnetization, the y-sensor response to the y-component alone, and the z-sensor response to the x- and z-components of magnetization. Like the *Constable and Parker* [1991] approach, that of *Oda and Shibuya* [1996] treats measurement errors as independent of position in the scan, and it includes an explicit term to minimize second differences in the deconvolved magnetization model. We develop two alternative algorithms in which we (a) include the full tensor response; (b) allow measurement errors to have systematic dependence on position; and (c) constrain the inverse calculations to minimize total model size rather than second differences. We use our new experimental results to observe the effects of each of these changes in processing approach, and find that despite the differences of algorithms and weighting factors, we

obtain very consistent magnetization models from each experiment.

2. Convolution and Deconvolution: Discrete Model

2.1. Forward Problem

[5] The data set consists of vectors $\vec{D}_1, \vec{D}_2, \cdots \vec{D}_n$ measured in positions 1 through n, which include "leader" and "trailer" positions extending beyond the top and bottom of the core. The magnetization distribution in the core is assumed to vary only in the z direction (along the core axis), and is represented in discrete form by the set of vectors $\vec{M}_1, \vec{M}_2, \cdots \vec{M}_m$; these are conventionally considered as the magnetizations of m infinitesimal-length volume elements spaced equally over the core length. It simplifies matters when the spacing between measurements equals that between model elements, and we follow *Constable and Parker* [1991] and *Oda and Shibuya* [1996] in making this simplification.

[6] Each measured vector $\vec{D}_i$ is a superposition of responses to all of the individual discrete-element magnetizations, plus an unknown error:

$$\vec{D}_i = \sum_{j=1}^{m} \mathbf{R}_{ij}\vec{M}_j + \vec{e}_i \qquad (1a)$$

The response function specifies the relationship between the magnetization vectors and the measurement vectors, and it is thus quantified as a set of second-rank tensors, which are not necessarily symmetric. The "equation of observation" [*Oda and Shibuya*, 1996] for the full data set is:

$$\begin{pmatrix} \vec{D}_1 \\ \vdots \\ \vec{D}_n \end{pmatrix} = \begin{pmatrix} \mathbf{R}_{11} & \cdots & \mathbf{R}_{1m} \\ \vdots & \ddots & \vdots \\ \mathbf{R}_{n1} & \cdots & \mathbf{R}_{nm} \end{pmatrix} \begin{pmatrix} \vec{M}_1 \\ \vdots \\ \vec{M}_m \end{pmatrix} + \begin{pmatrix} \vec{e}_1 \\ \vdots \\ \vec{e}_n \end{pmatrix} \qquad (1b)$$

or in compact form:

$$\mathbf{D} = \mathbf{RM} + \mathbf{e} \qquad (1c)$$

Each row of $\mathbf{R}$ specifies how the entire set of discrete-element magnetizations combine to produce a single measurement vector. Each column of $\mathbf{R}$ indicates how a single discrete-element magnetization contributes to the entire set of measurement vectors. The column matrices $\mathbf{D}$ and $\mathbf{M}$ contain respectively n and m elements, each of which is a 3-element column vector; they are computationally equivalent to column matrices with $3n$ and $3m$ scalar elements. Similarly the matrix $\mathbf{R}$, containing $n \times m$ elements, each of which is a 3×3 tensor, is "expanded" for subsequent computations into a $3n \times 3m$ matrix of scalar elements.

2.2. Inverse Problem

[7] When the instrument response function is sufficiently well known, a set of magnetization vectors $\mathbf{M}_{fit}$ can be calculated for a continuous-core data set $\mathbf{D}$ by least squares methods. We wish to find the set of best fit model parameters $\mathbf{M}_{fit}$ that minimizes $\chi^2 = \sum_{i=1}^{n} (|\vec{D}_i - \hat{D}_i|/\sigma_i)^2$ (where the $\hat{D}_i$ are best fit values calculated by convolution of $\mathbf{R}$ and $\mathbf{M}_{fit}$), and the σ_i are the individual measurement uncertainties (standard deviations). A direct least squares solution is

$$\mathbf{M}_{fit} = (\mathbf{r}^T\mathbf{r})^{-1}\mathbf{r}^T\mathbf{d} \qquad (2a)$$

where

$$\vec{d}_i = \vec{D}_i/\sigma_i \qquad (2b)$$

and

$$\mathbf{r}_{ij} = \mathbf{R}_{ij}/\sigma_i. \qquad (2c)$$

As is well known, however, this inverse calculation is ill-conditioned: it is strongly sensitive to even very small amounts of measurement noise, and it almost invariably results in $\mathbf{M}_{fit}$ models with wild down-core variations, unless additional constraints are imposed [*Constable and Parker*, 1991; *Oda and Shibuya*, 1994, 1996]. This numerical instability is an inevitable consequence of the geometry of the sensing coils and sample flux, and the resulting properties of $\mathbf{R}$. The columns of $\mathbf{R}$ represent the "basis functions" of the unmixing problem and the $\vec{M}$ values are the set of coefficients to be determined. Well-conditioned inverse problems have basis functions that are orthogonal (uncorrelated) or nearly so. For the deconvolution problem, the basis functions all have identical shapes, and each is shifted up or down with respect to the others. The shifts for neighboring columns are small compared to the response function width (otherwise deconvolution would be unnecessary); the higher the desired resolution, the stronger the correlation of adjacent columns (with smaller shifts and constant response function width) and the more ill-conditioned the inversion. Some form of additional constraint is therefore generally necessary to obtain a stable solution.

[8] An explicit smoothness constraint imposed by *Constable and Parker* [1991] and modified by *Oda*

and Shibuya [1996] produces for each data set a magnetization model that minimizes a weighted sum of squared misfits $\sum_{i=1}^{n} |\vec{D}_i - \hat{D}_i|^2$ and squared second differences $\sum_{j=2}^{m-1} |2\vec{M}_j - \vec{M}_{j-1} - \vec{M}_{j+1}|^2$. This form of constraint is particularly suitable because second differences represent linear combinations of model parameters that are relatively weakly constrained by the data; i.e., one can add an arbitrarily large multiple of $2\vec{M}_j - \vec{M}_{j-1} - \vec{M}_{j+1}$ to a magnetization model without producing correspondingly large changes in the predicted data set. However, second-difference constraints are not the only reasonable approach to stabilizing the inversion, and we will evaluate two alternative methods here. The real art in all of these constrained approaches is finding the optimal degree of constraint. A simple unconstrained least squares solution produces the smallest possible misfits, which are usually attained through extreme variations in the $\vec{M}(z)$ model. Progressively stronger second-derivative constraints yield larger misfits but magnetization models that are smoother. The tradeoff is optimized to produce the smoothest possible model with misfits that remain within the statistical uncertainty of the measurements [*Constable and Parker*, 1991; *Oda and Shibuya*, 1996; *Guyodo et al.*, 2002]. In the formulation of *Oda and Shibuya* [1996] the optimization involves repeated least squares minimization of the quantity

$$S = \sum_{i=1}^{n} |\vec{D}_i - \hat{D}_i|^2 + u^2 \sum_{j=2}^{m-1} |2\vec{M}_j - \vec{M}_{j-1} - \vec{M}_{j+1}|^2 \quad (3)$$

using different values of the smoothing hyperparameter u, calculating a Bayesian probability-related parameter (ABIC) for each solution, and using that quantity to determine the optimal u and best overall magnetization model.

[9] In both of these pioneering papers [*Constable and Parker*, 1991; *Oda and Shibuya*, 1996] measurement uncertainties were considered to be dominated by high-frequency Gaussian noise (after taking care of recognizable and correctable errors due to flux jumps and individual noise spikes [*Oda and Shibuya*, 1996]). Random error magnitudes were assumed to be independent of z ($\sigma_i = \sigma$). Here we explore two simple alternative deconvolution approaches that allow us to incorporate different descriptions of measurement error and to evaluate their effects. These simple approaches produce reasonably smooth models without explicit second-derivative constraints, and we show experimentally

that they yield results having accuracy comparable to that of the ABIC calculations. The first is based on singular value decomposition (SVD) [e.g., *Press et al.*, 1986]. SVD decomposes **r** (or more generally, the design matrix of any linear inverse problem) into the product of a column-orthogonal matrix **U**, a diagonal matrix **w**, and a row-orthogonal matrix $\mathbf{V}^T$; the diagonal elements of **w** are the "singular values." Columns of **V** represent a set of orthogonal vectors spanning the solution space, and the corresponding singular values in effect measure the resolvability of those vectors. For example, in an underdetermined inverse problem, where the number of unknowns exceeds the number of linearly independent equations, at least one of the singular values is zero, and the corresponding column(s) of **V** represent the "null space" of the inversion: linear combinations of parameters that can be added to a model without changing predicted data values at all. In such cases an infinite number of exact solutions exist, and SVD-based inversion techniques return the smallest solution vector, i.e., the one that minimizes the sum of squared parameter values. In overdetermined problems, such as the deconvolution problem, small singular values correspond to linear combinations of parameters that are only weakly resolvable, i.e., combinations that when added to a model produce only slight changes in predicted data. These can be "zeroed out" in the calculation of the best fit model, resulting in a slight increase in misfit but producing a smoother model (as measured by total length of the solution vector). As in the case of second-derivative constrained inversion, the optimal degree of filtering produces the smoothest model that still has misfits within the expected measurement error. We can specify the degree of smoothing in terms of the zeroing threshold ζ: a singular value w_i is set to zero when $w_i/w_{max} < \zeta$. Larger values of ζ produce smoother models and larger misfits.

[10] The second alternative approach that we investigate here is regularized least squares (RLS), specifically Tikhonov-Phillips regularization, which is related to the Levenberg-Marquardt method of nonlinear inversion [e.g., *Hansen*, 1998]:

$$\mathbf{M}_{fit} = (\mathbf{r}^T\mathbf{r} + \Gamma^T\Gamma)^{-1}\mathbf{r}^T\mathbf{d} \quad (4)$$

The Tikhonov matrix Γ is of a form chosen to impose certain properties on the solution; for $\Gamma = \alpha \mathbf{I}$ (where **I** is the identity matrix and α is a damping parameter) the calculation favors solutions with small norms. Increasing the diagonal dominance of $\mathbf{r}^T\mathbf{r}$ in effect causes the calculation to treat the basis

functions as more orthogonal, reducing their interchangeability and stabilizing the inversion. Once again the crux of the problem is to find an optimal solution by appropriate choice of smoothing level. ABIC minimization is rigorous but not simple to adapt, so we consider two simple alternative ways to define the optimum. First, we can find the simplest model (smallest mean square parameter values or second differences) that fits the data to within a specified tolerance [*Constable and Parker*, 1991]. According to *Oda and Shibuya* [1996], this method can become unstable if the error tolerance is inaccurately specified. The second approach, and the one that we use for both SVD and RLS, is based on the trade-off between fitting errors and smoothness. We obtain a set of solutions with differing levels of damping (ζ and α), calculate total misfit and model size, and plot them on a tradeoff curve (as done for example by *Parker and Gee* [2002]). The tradeoff is favorable when the slope is steep (model size is reduced rapidly with small increases in misfit) and becomes unfavorable when the slope shallows. The "knee" in the tradeoff curve, where its slope changes sharply, corresponds to the optimal model. This is equivalent to minimizing a weighted sum of model size and misfit, analogous to equation (3).

[11] SVD optimization is very efficient; the design-matrix decomposition is performed once, and the "backsubstitution" calculations with different zeroing thresholds (ζ) involve only straightforward matrix multiplication. A relatively large number of thresholds can therefore be used to define the tradeoff curve. For small ζ, the SVD calculations yield results identical to those generated by direct least squares solution (equation (2)), i.e., they give the best possible fit but contain unrealistically large downcore variations in magnetic direction and intensity. Zeroing of progressively larger singular values prior to backsubstitution initially results in sharp decreases in model size (as measured, e.g., by root-mean square (rms) moment) with relatively little degradation of the fit. Eventually ζ becomes too large and the inversion is overdamped, producing excessively smooth models with significant lack of fit to the measured data. Optimization of the RLS inversions works in the same way, but is much more time-consuming, because the matrix inversion must be performed for each value of the damping parameter α. Precise definition of the knee location on the tradeoff curve would be most rigorously done through something like the Bayesian analysis of *Oda and Shibuya* [1996], but we settle for a simple alternative, which we have found by trial and error to work satisfactorily: we

increase the damping parameter (ζ or α) in systematic steps, calculating the model size M_0 (mean square magnetization intensity) and misfit ε (mean square residual) for each step, and define the knee as the point where $d(\log(M_0))/d(\log(\varepsilon))$ first exceeds -0.2.

2.3. Estimates of Parameter Uncertainty

[12] The matrix $\mathbf{C} = (\mathbf{r}^T\mathbf{r})^{-1}$ (or, for RLS, $(\mathbf{r}^T\mathbf{r} + \mathbf{\Gamma}^T\mathbf{\Gamma})^{-1}$) gives the variances and covariances of the model parameters. The standard deviations for the parameter estimates are therefore given by $\sigma(M_j) = \sqrt{C_{jj}}$ and the 95% confidence interval is $M_{fit,j} \pm 1.96\sigma(M_j)$.

3. Response Function Determination and Noise Characterization

3.1. Response Function

[13] The response function is determined primarily by the geometry of the sensing coils and by that of the superconducting shield, which affects the geometry of the magnetic flux due to the sample [*Zięba*, 1993; *Shibuya and Michikawa*, 2000]. The axial (z) coils are circular, with a diameter of ~85 mm, and the transverse sensors are saddle-coil pairs, formed on the same cylindrical core. In our u channel magnetometer (2G model 755–1.65) the axial-coil pair separation is $\Delta = 24$ mm, and the saddle coils have a length L ~ 68 mm. This geometry is intermediate between the "high homogeneity" arrangement ($\Delta = 40$ mm, L ~ 100 mm) optimized for discrete-sample measurements and the "high-resolution" geometry ($\Delta = 10$ mm, L ~ 40 mm) designed for maximum resolution of downcore variations. Although the coil geometry is accurately known, calculation of the instrument response function from first principles is strongly complicated by "image effects" related to the superconducting shield [*Zięba*, 1993; *Shibuya and Michikawa*, 2000; *Parker and Gee*, 2002]. Our magnetometer uses pulse-tube cryocooling rather than a liquid helium reservoir. The distinction is important here because the geometry of the superconducting shield in the "dry" instruments is different than that in the conventional liquid-filled magnetometers, and the instrument response function consequently differs in subtle ways (B. Goree, personal communication, 2005) that nevertheless are critical for accurate deconvolution.

[14] Empirical determination of the instrument response is most simply and commonly determined

by direct measurement. A thin slice of uniformly magnetizable material, having the same cross-sectional dimensions as those of a u channel sample, is magnetized precisely along each axis (x, y and z) in turn and measured in "continuous" scans (e.g., at 5-mm intervals) over a range extending at least 10 cm either way from the center of the sensing coils. This shows directly how (for example) the x-coils respond to the y-component of magnetization, as a function of sample position.

[15] Small errors in orienting and positioning the response-calibration sample can adversely affect the repeatability and accuracy of the determination. Ideally the response function should be characterized by fitting physically constrained functions (e.g., harmonic splines satisfying Laplace's equation [*Parker and Gee*, 2002]) to a set of detailed but necessarily inexact measurements. We have settled for an intermediate expedient, fitting by the same sort of SVD and RLS methods that we use for deconvolution.

[16] Equation 1 applies equally well to (a) the conventional measurement and deconvolution problem, in which we know **R** and measure **D** to determine **M**, and (b) the calibration problem, in which we know **M** and measure **D** to determine **R**. In the latter case, additional columns can be added to **M** to specify magnetizations in differing controlled orientations, and the corresponding measurements can be entered in additional columns of **D**. Calculating **R** by least squares is then rather similar to calculating a conventional single-specimen magnetic anisotropy tensor. Including data from a significant number of scans helps to average out noise and positioning errors.

[17] We have computed the response function from six scans (32-cm length, 1-mm spacing) of a homogeneous specimen with dimensions of $18 \times 18 \times 15$ mm³ (i.e., the same cross-sectional dimensions as a u channel), with differing magnetization directions (Figure 1a). The calculated response function (Figure 1b) shows substantial similarities to those obtained for liquid-reservoir instruments [e.g., *Oda and Shibuya*, 1996; *Guyodo et al.*, 2002; *Parker and Gee*, 2002]. The axial response $R_{ZZ}(z')$ (i.e., the z-sensor response to the z component of magnetization, as a function of measurement position z') features twin peaks, corresponding to the individual axial coils, with a separation of 24 mm. The transverse response elements $R_{XX}(z')$ and $R_{YY}(z')$ are single-peaked, with a width at half-maximum (~77 mm) comparable to that of $R_{ZZ}(z')$ and slightly wider than the

length of the saddle coils (69 and 68 mm respectively). The transverse response curves differ significantly for the liquid-free instrument, however, in their asymmetry: negative lobes occur only on one side, as a result of the changed arrangement of superconducting shields in the "dry" instrument. As in previous studies, the largest cross terms are z-x and x-z, with odd symmetry and peaks near the ends of the saddle coils. Like *Parker and Gee* [2002] we also find non-negligible x-y terms with even symmetry and y-z terms with approximate odd symmetry. These cross terms can arise when core samples have asymmetrically shaped cross-sections (e.g., split cylindrical cores with semicircular section), or for symmetrically shaped cores (e.g., u channels with square or rectangular section) when the geometric axis of the u channel does not exactly coincide with that of the sensing coils [*Shibuya and Michikawa*, 2000; *Parker and Gee*, 2002].

3.2. Noise Characterization

[18] We wish to find the smoothest possible model that can reproduce the measured data to within their statistical uncertainty, and therefore we begin by considering the sources of error and their potential magnitudes. Quantification of the uncertainty in each measurement can be accomplished directly by repeating each scan multiple times, but because of the time required this is rarely done, and errors are assumed to be dominated by random noise (normal distribution with zero mean and variance σ^2, and independent of position, i.e., serially uncorrelated). Measurement positions are assumed to be known exactly, but inaccuracies at some level are inevitable and can add to the "noise" when signal strength changes as a function of position. *Oda and Shibuya* [1996] evaluated the possible importance of positioning errors in a data set by comparing the fitting errors for successive scans (after different alternating-field (AF) demagnetization levels), and concluded that they were negligible. However, *Guyodo et al.* [2002], by combining multiple replicate scans in differing orientations, concluded that positioning errors of up to a few mm can occur due stick-slip behavior of the u channel transport belt on the track and elasticity of the Kevlar string connecting the belt to the stepper motor. They stated that in regions of high gradients in measured magnetizations, these positioning errors are equivalent to measurement errors of a few percent. For strongly magnetic u channels, this may be the dominant source of error, especially near the ends and other regions of strong signal gradient. In
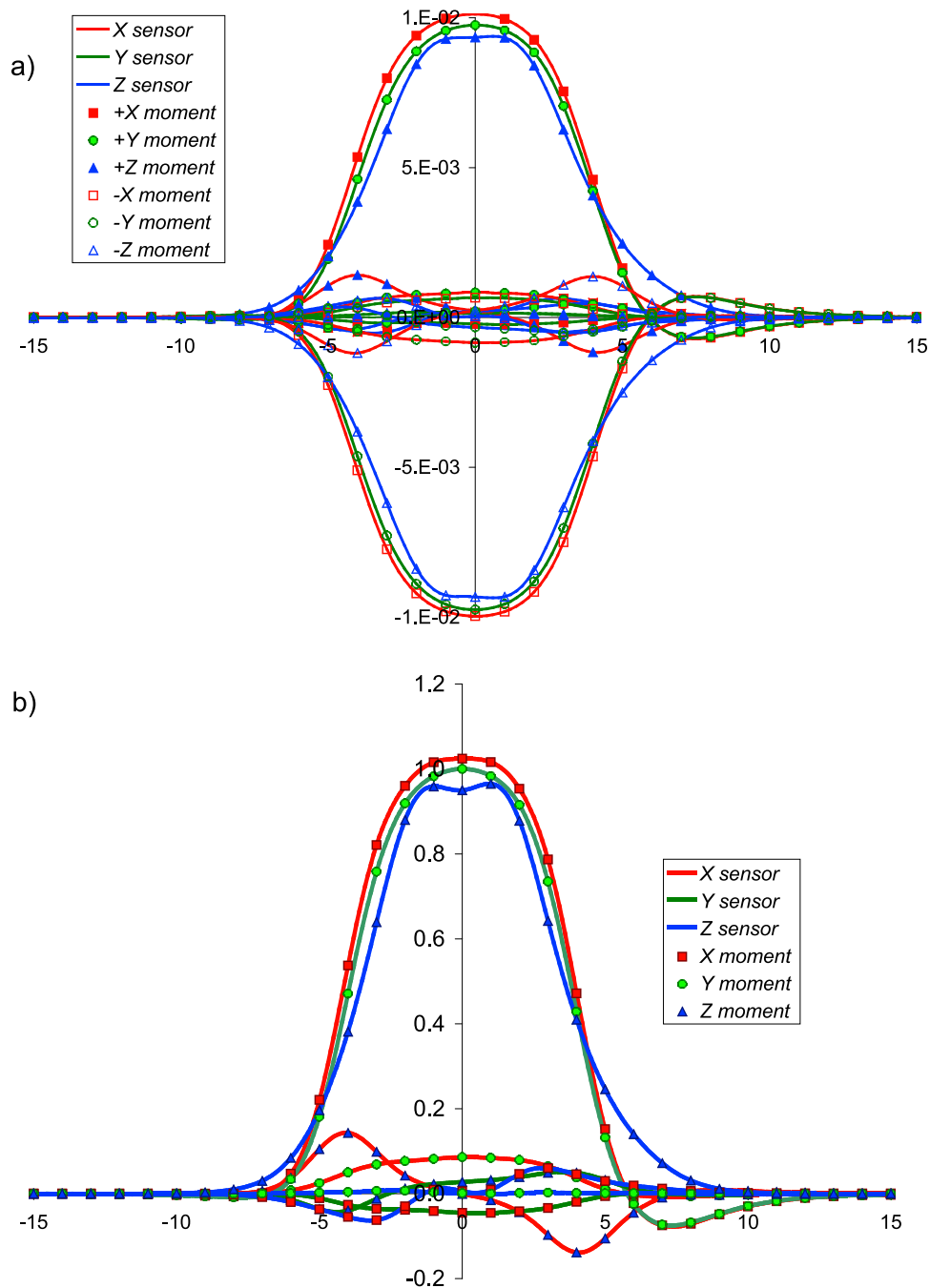
Figure 1. (a) Response function calibration data for the "helium-free" magnetometer: red, green and blue curves respectively show the X, Y and Z magnetometer responses to magnetic moments oriented in the x (red squares), y (green circles) and z (blue triangles) directions. Solid and open symbols refer to positive and negative moments, respectively. (b) Response function of the "helium-free" magnetometer calculated from the data in Figure 1a.

addition to the random errors related to individual-position imprecision, systematic positioning errors can also be introduced by inexact placement of the u channel sample onto the track. Other significant error sources include those that directly affect the measurements (primarily instrument noise and uncompensated drift) and those that affect the deconvolution calculations (e.g., errors in the response function, or lateral heterogeneity of the magnetization (variation in the x-y plane)) [*Oda and Shibuya*, 1996].
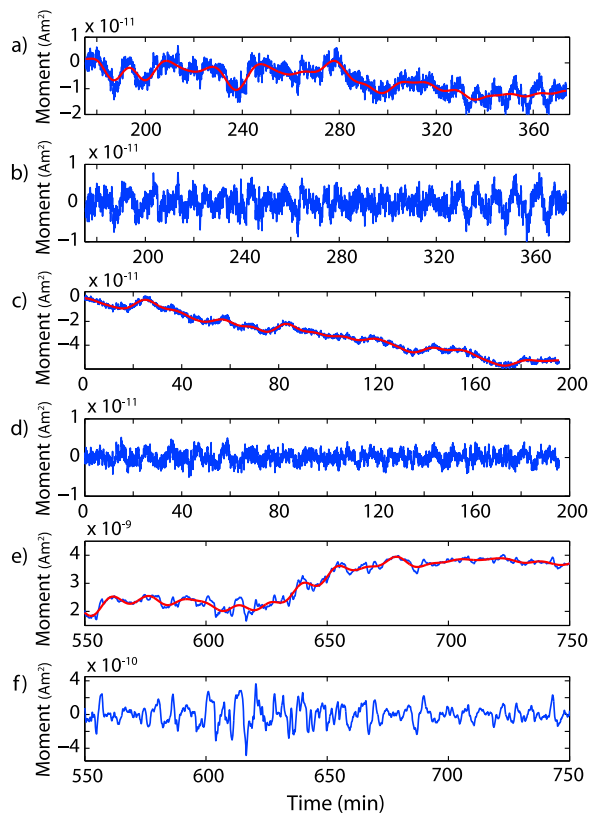
Figure 2. Examples of single-axis SQUID noise measured on the IRM's 2G Long Core magnetometer. (a and b) X SQUID and (c and d) Z SQUID measured during a period of instrumental quiescence. (e and f) Y SQUID measured with instrument in non-ideal state. Red curve is long-wavelength signal (periods >10–15 min) associated with timescales longer than that required to measure a complete core. This signal has been removed from Figures 2b, 2d, and 2f. Note that *y* axis scales vary over 2 orders of magnitude between plots.

[19] Instrument noise, involving a spectrum of periodicities, will clearly vary from instrument to instrument, as well as from day to day or from hour to hour on the same instrument. For this reason *Constable and Parker* [1991] quantified noise using measurements at the beginning and end of a scan, with the core outside the sensing region. Examples of "good day" instrumental noise measured on the IRM's 2G Long Core magnetometer are shown in Figures 2a–2d; short periods (<45 s) are typically dominated by white noise with amplitudes less than a few times 10^{-12} Am^2, while longer periods display the characteristic 1/f noise common to most DC SQUID systems [e.g., *Clarke*, 1993]. The instrument commonly enters a state of increased noise and drift (Figures 2e and 2f), presumably related to trapped flux somewhere in the

SQUID system, following measurement of relatively strong (>10^{-5}Am^2) signals; both short- and long- period variations are one or two orders of magnitude greater than in the quiescent state. When such a noisy state is recognized, it can typically be remedied by warming the SQUIDs or the stripline to release the trapped flux. However, if the instrument enters a high-noise state during a long automated sequence of demagnetization steps, numerous noisy scans may result.

[20] Longer-period (>1 min) variations are generally larger in amplitude than those with shorter periods (Figures 2 and 3), and are potentially more problematic because they may not average to zero over significant areas of a u channel scan. Variations with very long periods, much greater than the time scales associated with measuring a core (t_{scan} ~ 10–15 min), can be removed from a scan with sufficient accuracy by linear drift correction,
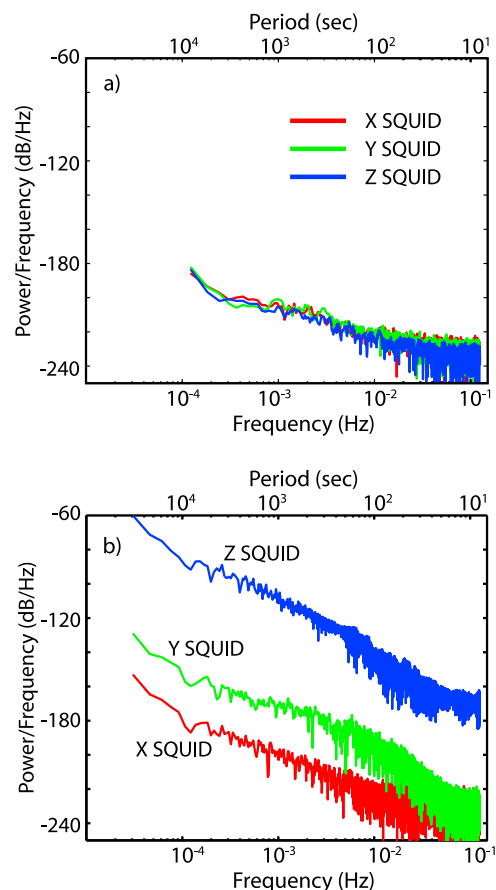

Figure 3. Power spectral density estimates of SQUID noise measured (a) during an instrumental quiescent period and (b) during a non-ideal state. Note that on timescales relevant to core measurement (>~30 s), the noise spectrum is dominated by 1/f noise.

but intermediate-period drift produces serially correlated errors that can be difficult or impossible to distinguish from meaningful data variations, unless replicate scans are measured. After high-pass filtering of a noise-measurement set to remove the long-period drift (red line in Figures 2a, 2c, and 2e), remaining variations with amplitudes of $1-2 \times 10^{-11}$ Am^2 are not uncommon in instrumental quiescent mode (Figures 2b and 2d), and they are at least order of magnitude larger in non-ideal states (Figure 2f). This type of intermediate-period background variation might be termed instrumental drift, but it is typically nonlinear, unpredictable, and impossible to correct. If we define "time-integrated drift" as the difference between the background measurement before and after the sample scan, one approach is to discard measurement scans where the time-integrated drift is >1–3% of the minimum sample signal strength. However, because of the often oscillatory nature of the noise (e.g., Figure 2b from 320 to 380 min), this precaution may not prevent considerable intermediate-period noise from passing undetected into the data.

[21] In general, maintaining a sufficiently high signal/noise ratio is most difficult for very weakly magnetic samples or for core samples that have large variations in magnetic intensity. For very weak cores, the major limitation is the instrumental background noise as discussed above. Strongly magnetic samples (or portions of core samples) tend to increase long-period noise (e.g., Figures 2e, 2f, and 3b) which may not be a problem for the highly magnetic sections themselves, but could create issues for weaker core sections which cannot be measured separately. The measurement of *very* strong cores (>a few times 10^{-5} Am^2) may lead to multiple flux jumps or extreme noise on the order of the measured moment (e.g., Figure 3b, Z SQUID). These cores can be virtually impossible to measure, let alone deconvolve.

4. Synthetic and Natural Samples and Experiments

[22] For experiments with controlled magnetization distributions we manufactured an artificial sample set by filling a standard u channel (18 mm × 18 mm interior dimensions), approximately 28 cm long, with hydraulic cement and letting it harden. The hardened cement is very homogeneous and contains fine-grained ferrimagnetic oxides in sufficient quantity to acquire strong, stable and spatially

uniform anhysteretic remanence (ARM), with intensities of ~1 A/m produced by a DC field of 50 μT and an AC field of 100 mT. Its properties are quite similar to those of the Pozzolana cement described by *Sagnotti et al.* [2003]. After curing, we removed the solid block from the u channel and sliced it into segments of approximately 2 cm length, using a water-cooled diamond-blade saw. These blocks can be magnetized anhysteretically in an offline AF instrument in any desired orientation and in DC and AC fields selected to control the intensity of ARM acquired. The segments can be measured individually as discrete specimens and then replaced in the u channel for measurement as a continuous core sample with known magnetization distribution, similar to the "train of cubes" experiment [*Weeks et al.*, 1993; *Roberts*, 2006]. The reassembled sample length is 27.3 cm, as some material was removed by sawing.

[23] Three initial experiments involved ARMs with uniform intensities and varying degrees of directional variation. In experiment 1, small directional variations were produced by roughly aligning the segment z axes with the AF axis, and introducing random deliberate misalignments of up to ~30°. Experiment 2 magnetizations were imprinted roughly along the specimen y axes, again with random small misorientations, and with one segment rotated by approximately 90°, magnetized roughly along the z axis, to simulate a short field excursion record, not unlike those in the work by *Guyodo et al.* [2002]. In experiment 3 the ARMs were primarily in the x direction, with two short "excursions" (single segments magnetized in the y and z directions) and one short reversed interval (a single segment magnetized in the -x direction), as in the experiment of *Weeks et al.* [1993]. In each of these experiments the reassembled u channel was measured three times, to enable quantification of measurement variability.

[24] A separate experiment was carried out to evaluate the accuracy of the deconvolution approaches for magnetizations varying in intensity downcore, with little directional change. This used a natural lake sediment core from Deming Lake, Minnesota. The 98-cm core section, STD2-DEM07-5A-4B-1 (referred to as 4B hereafter), is composed of sandy-silty clay with up to 40% organic matter. Section 4B was chosen for the experiment based on the variability of its magnetic susceptibility record, measured at the National Lacustrine Core Repository (LacCore) using core
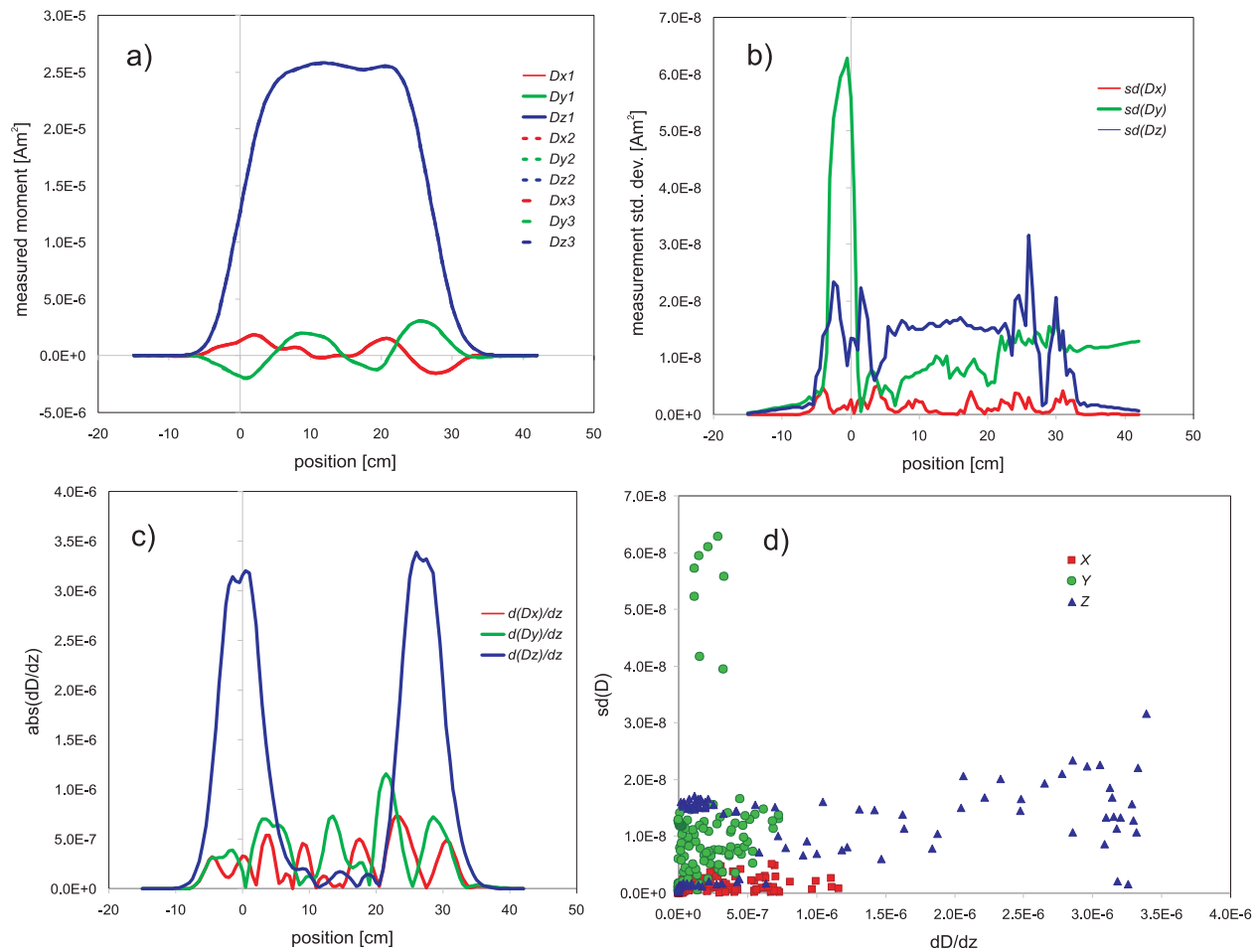
Figure 4. (a) Measured data for experiment 1; red, green and blue respectively correspond to x y and z components. Three independent scans show excellent reproducibility - differences between scans are indistinguishable in the plot. (b) Standard deviation of measured x, y and z components. (c) Downcore gradients of the measured x, y and z components. (d) Correlation of standard deviations and gradients of measured data.

logger sensors. The section was subsampled at 2 cm intervals after completion of u channel IRM acquisition experiments.

5. Results

5.1. Synthetic Sample

[25] In each of the cement u channel experiments, the three replicate runs show very high signal/noise ratios and quite good repeatability (Figures 4a, 5a, and 6a). Standard deviations (Figures 4b, 5b, and 6b) are typically less than 0.5% of the mean values, but nevertheless are quite high (a few times 10^{-8} Am^2) compared to random high-frequency noise (typically of order 10^{-12} to 10^{-11} Am^2, section 3 above). The measurement errors are clearly not independent of position: sharp peaks in the standard devi-

ation generally occur at points of maximum slope in the measured $\vec{D}(z)$ curves (compare Figures 4b, 4c, 5b, 5c, 6b, and 6c), showing that the variability between replicate measurements is primarily due to small positioning errors rather than to SQUID noise or drift. Because a positioning error Δz directly affects the measurements according to $\Delta \vec{D} = (d\vec{D}/dz)\Delta z$, we plot the standard deviations of the replicate measurements against data gradients in Figures 4d, 5d, and 6d, showing very strong correlation in experiment 2 (Figure 5), moderate correlation in experiment 3 (Figure 6), and rather weak correlation in experiment 1 (Figure 4). In the experiment 2 results (Figure 5d), the slopes for the x, y and z components all correspond to a position-error standard deviation of 0.20 mm, and the intercepts correspond to instrument noise of 6 × 10^{-10} (z) to 1.4 × 10^{-9} (x) Am^2. An appropriate
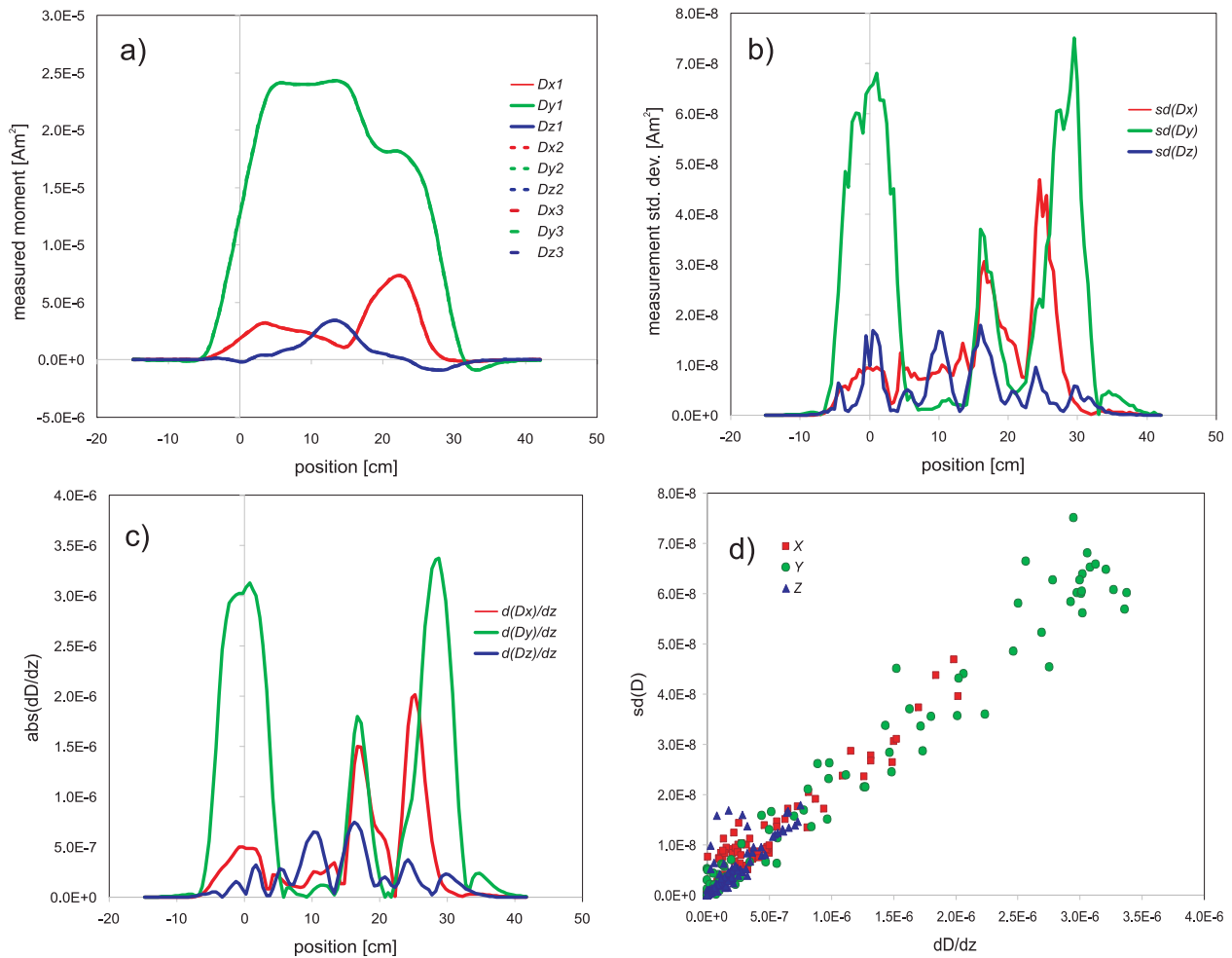
Figure 5. (a) Measured data for experiment 2; red, green and blue respectively correspond to x y and z components. Three independent scans show excellent reproducibility. (b) Standard deviation of measured x, y and z components. (c) Downcore gradients of the measured x, y and z components. (d) Correlation of standard deviations and gradients of measured data.

description of measurement errors in this data set is therefore

$$\vec{\sigma}_D(z) = \vec{\sigma}_0 + \sigma_z d\vec{D}/dz, \qquad (5)$$

with $\vec{\sigma}_0$ comprising noise on all time scales short enough to persist in the data set after linear drift correction, and the positional standard deviation σ_z equal to 0.02 cm. In experiment 1, even though the reproducibility of the measurements appears to be nearly perfect (Figure 4a), and both the data and the gradients smoothly approach zero in the "leader" and "trailer," there is significant variance in this data set that is not explained either by positioning errors or by short-period noise, and we attribute it to intermediate-period drift, for which no simple $\sigma_D(z)$ description can be specified. The experiment 3 results show a combination of short-period noise,

intermediate-period drift and positioning errors. Slopes for the x, y and z components correspond to a position-error standard deviation of 0.10 mm in each case, and the intercepts correspond to instrument noise of 4×10^{-10} (z) to 3×10^{-9} (x) Am^2.

[26] The discontinuous changes in magnetization intensity at the u channel ends, and the sharp directional changes in experiments 2 and 3 (Figures 8–10), are strongly smoothed in the continuously measured data sets, as expected (Figures 4a, 5a, and 6a). The 90-degree directional change in experiment 2 at z ~ 21 cm is shown by a small peak in M_x at that location and a decrease in M_y that persists through the rest of the core due to the convolved effects of the directional change and the core end. The rapid sequence of directional changes in experiment 3 between 7 and 15 cm
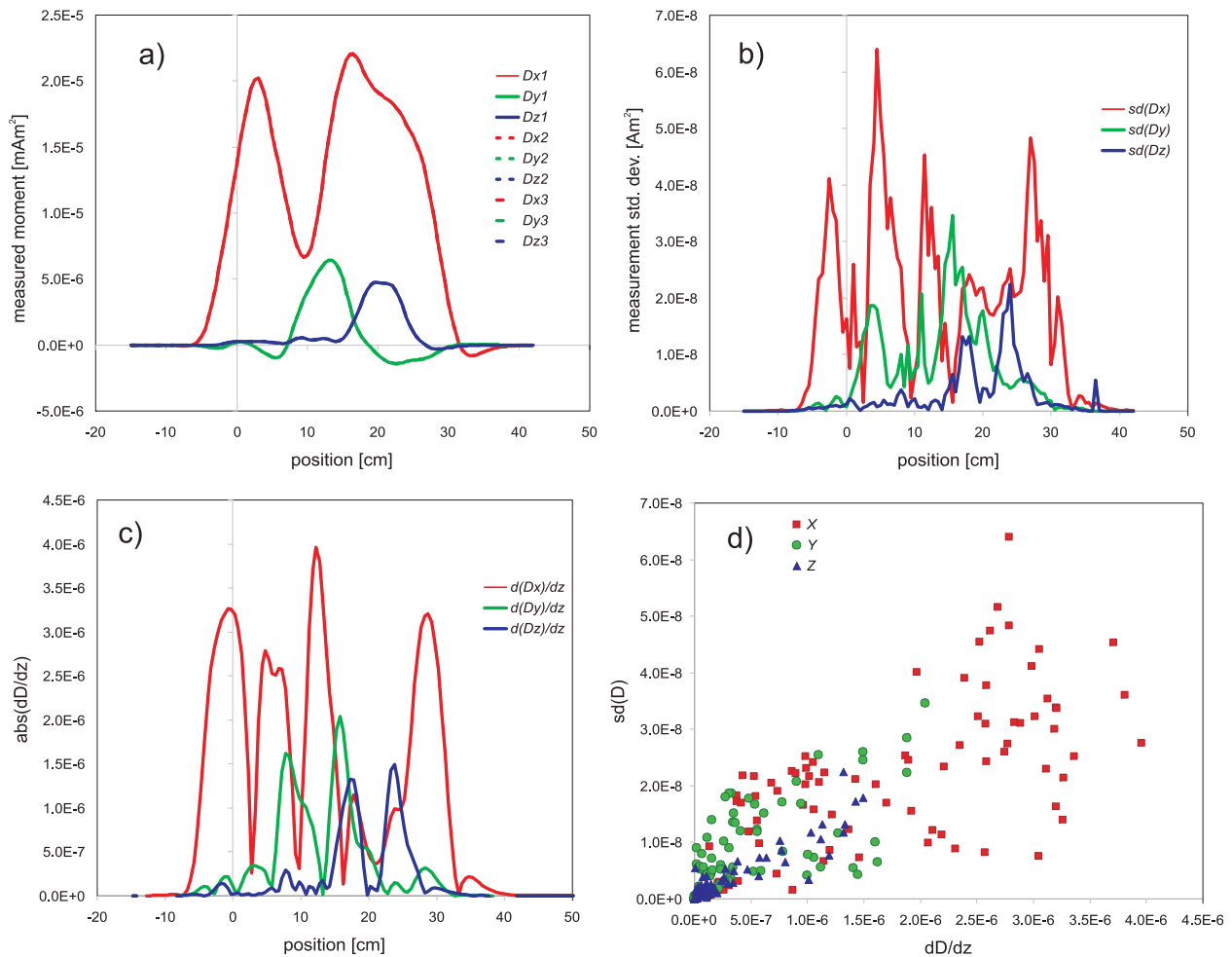
Figure 6. (a) Measured data for experiment 3; red, green and blue respectively correspond to x y and z components. Three independent scans show excellent reproducibility. (b) Standard deviation of measured x, y and z components. (c) Downcore gradients of the measured x, y and z components. (d) Correlation of standard deviations and gradients of measured data.

results in a single smooth minimum in M_x at around 10 cm.

[27] The optimal damping level for of the inverse calculations is in all cases quite well defined by a sharp break in slope on the tradeoff curve (Figure 7). Deconvolution using the assumption of position-independent measurement errors produces remarkably good estimates of the true magnetization distribution in each of the experiments, using all three methods (Figures 8–10). The full amplitude of the directional-component variations is accurately reconstructed, with relatively little spurious oscillation. The specious variations that do occur are primarily within a few centimeters of the core ends or other abrupt changes in directional-component intensity, and they are slightly larger for the ABIC-minimized models than for the SVD and

RLS models, perhaps because we use the full response tensor for the latter two. Changing the estimated measurement error σ_D does not affect the deconvolved magnetization models. However, the estimated parameter uncertainties σ_M do scale in proportion to σ_D [see, e.g., *Oda and Shibuya*, 1996, equation 18].

[28] These experiments provide a best-case scenario for the inverse calculations because of the high signal/noise ratio (mostly >1000) and the relatively dense sampling (5-mm steps). It is of interest to simulate less favorable situations, by adding random noise to the data (as in the work by *Oda and Shibuya* [1996]) and by using subsets of the data resampled at lower resolution. When we reduce signal/noise ratios by adding Gaussian-distributed random deviates to the measured data of
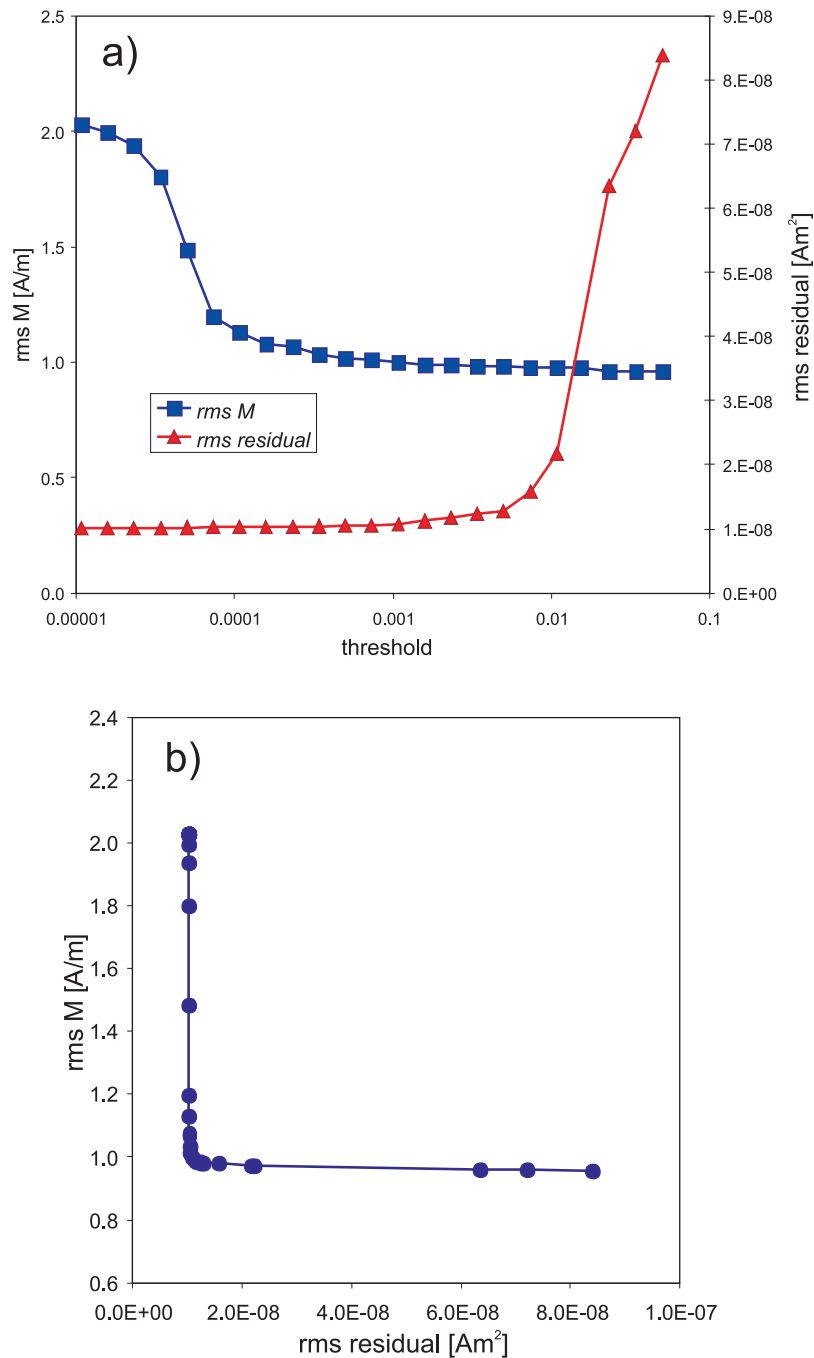
Figure 7. (a) Effect of different zeroing thresholds for SVD, for the data of experiment 2. The ratio w_{min}/w_{max} ~ 1e-5, so thresholds below this yield models identical to the simple least squares solution. Higher zeroing thresholds first decrease the model size (~50% reduction in RMS moment) with minimal increase in misfit; thresholds above 1e-2 significantly degrade the fit. (b) The optimal model is determined by the location of the "knee" in the tradeoff curve.

experiment 3, the different optimization techniques all respond in essentially the same way, increasing the model smoothness and reducing resolution and accuracy accordingly. Synthetic noise with a standard deviation of 5×10^{-8} Am^2 (signal/noise ~ 500) results in models (Figures 11a and 11b) in

which the directional-component variations are still accurately located but their full amplitude is not recovered; spurious variations are confined to the same small amplitudes observed in the clean-data inversions. A further tenfold increase in noise levels (signal/noise ~ 50) seriously degrades the
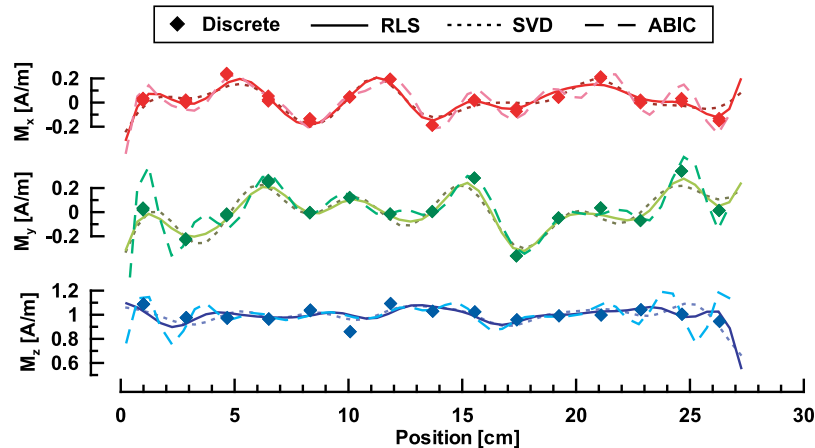
Figure 8. The u channel magnetization distribution for experiment 1. Diamonds show measured values for discrete segments; curves show x, y and z components of magnetization models obtained by deconvolution of continuous-channel measurements, using SVD, RLS and ABIC minimization as indicated.

resolution and accuracy of the models (Figures 11c and 11d): the directional-component variations are reduced to about half their true values, and the double minimum in the x component near 10 cm is no longer resolved into separate features. Calculated confidence intervals (not shown) are large enough to include the variability in the set of models, but often exclude the true directional-component magnetizations.

[29] The directional-component variations in these experiments have a characteristic length scale of two centimeters. Not surprisingly, some "over-sampling" is necessary to obtain good resolution of

the rapidly varying magnetization directions in experiment 3. Measurements in steps of 1 cm still yield excellent resolution (Figure 12a), but another twofold increase in step size results in significant loss of detail in the magnetization models (Figure 12b). Because of the explicit second-difference minimization in the ABIC approach, we expected the down-up-down-up sequence in M_x to be suppressed more than it is for the SVD and RLS models, but in fact there is no real difference: in all cases the amplitudes of the directional-component variations are reduced significantly from their true values. Despite the high signal/noise ratio, the
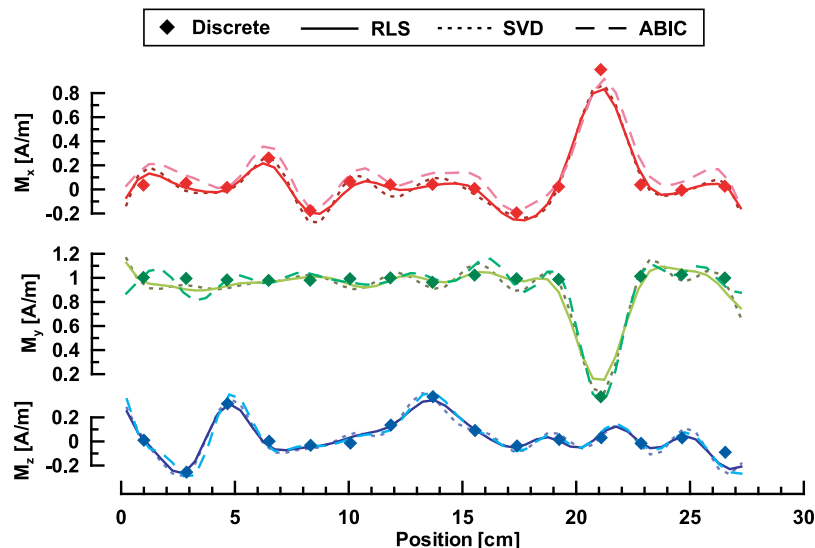

Figure 9. The u channel magnetization distribution for experiment 2. Diamonds show measured values for discrete segments; curves show x, y and z components of magnetization models obtained by deconvolution of continuous-channel measurements, using SVD, RLS and ABIC minimization as indicated.
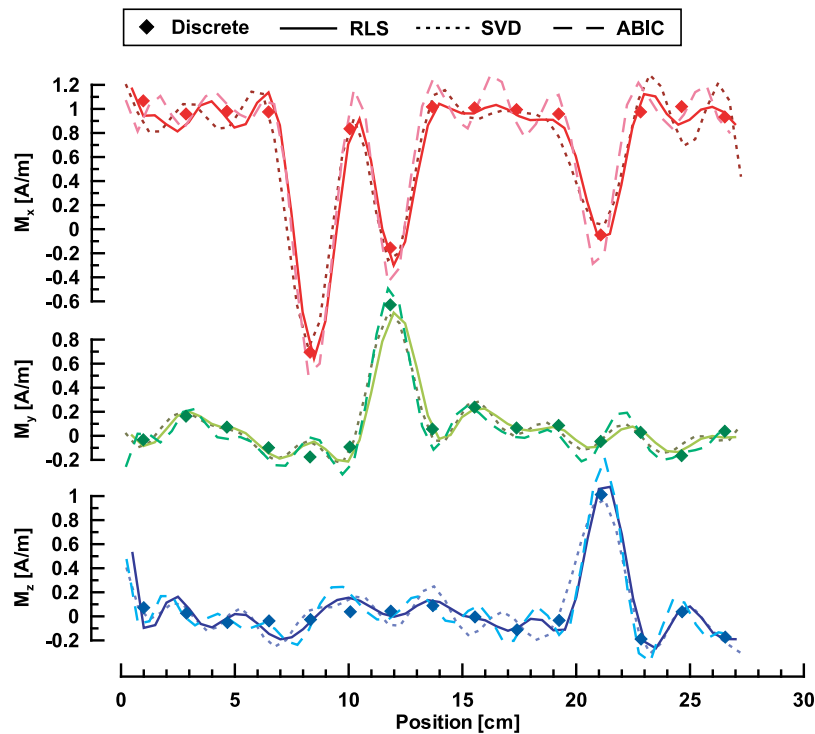
Figure 10. The u channel magnetization distribution for experiment 3. Diamonds show measured values for discrete segments; curves show x, y and z components of magnetization models obtained by deconvolution of continuous-channel measurements, using SVD, RLS and ABIC minimization as indicated.

solutions for this critical sampling density (measurement interval = length scale of magnetic variations) quite strongly resemble those obtained from the oversampled data set with s/n reduced to 50 by the addition of synthetic noise (compare Figures 12b, 11c, and 11d).

[30] When we attempt to account for position-dependent measurement errors in a more accurate way, i.e., by using equation (5) in equations (2b) and (2c), the results are rather surprising. First for comparison we show in Figure 13a the best fit model obtained by SVD with a fixed (position-independent) measurement-error probability distribution, with zero mean and $\sigma_D = 1 \times 10^{-8}$ Am^2 for x, y and z. The best fit model is independent of the specified error variance when σ_D does not vary with depth; a fixed σ_D affects only the estimated parameter uncertainties. Therefore we first find the best model, calculate its RMS residual, and then use that as an estimate of σ_D to obtain the confidence intervals (as done by *Oda and Shibuya* [1996]). Both the model and the error bars are very similar to those calculated by the ABIC code (not shown). Residuals (Figure 13b) exhibit no systematic variation with depth in the constant-σ_D case. In contrast, the same data set deconvolved by SVD with a depth-

dependent measurement error model (equation (5), with the x, y and z components of $\vec{\sigma}_0$ each equal to 2×10^{-10} Am^2, and $\sigma_z = 0.02$ cm) yields a calculated magnetization distribution (Figure 13c) that differs in some significant ways from the constant-σ_D model. In particular, the x and z components of the deconvolved magnetization show significantly sharper (higher frequency and amplitude) variations for z < 5 cm, and the y component has more variability over the entire length. The 95% confidence intervals reflect the increased measurement uncertainties, and include almost all of the magnetization values determined by discrete-specimen measurements. The residuals for this inversion (Figure 13d) show exactly the expected downcore variation, in accord with the specified measurement uncertainties, with relaxed fitting tolerance in areas of high signal gradient. What is surprising is that in the area where the fitting tolerance is most relaxed (z < 5 cm), the model contains the largest and most erratic variations.

5.2. Lake Sediment Sample

[31] The pulsed-field IRM has minimal directional variation (measured vectors for the continuous u
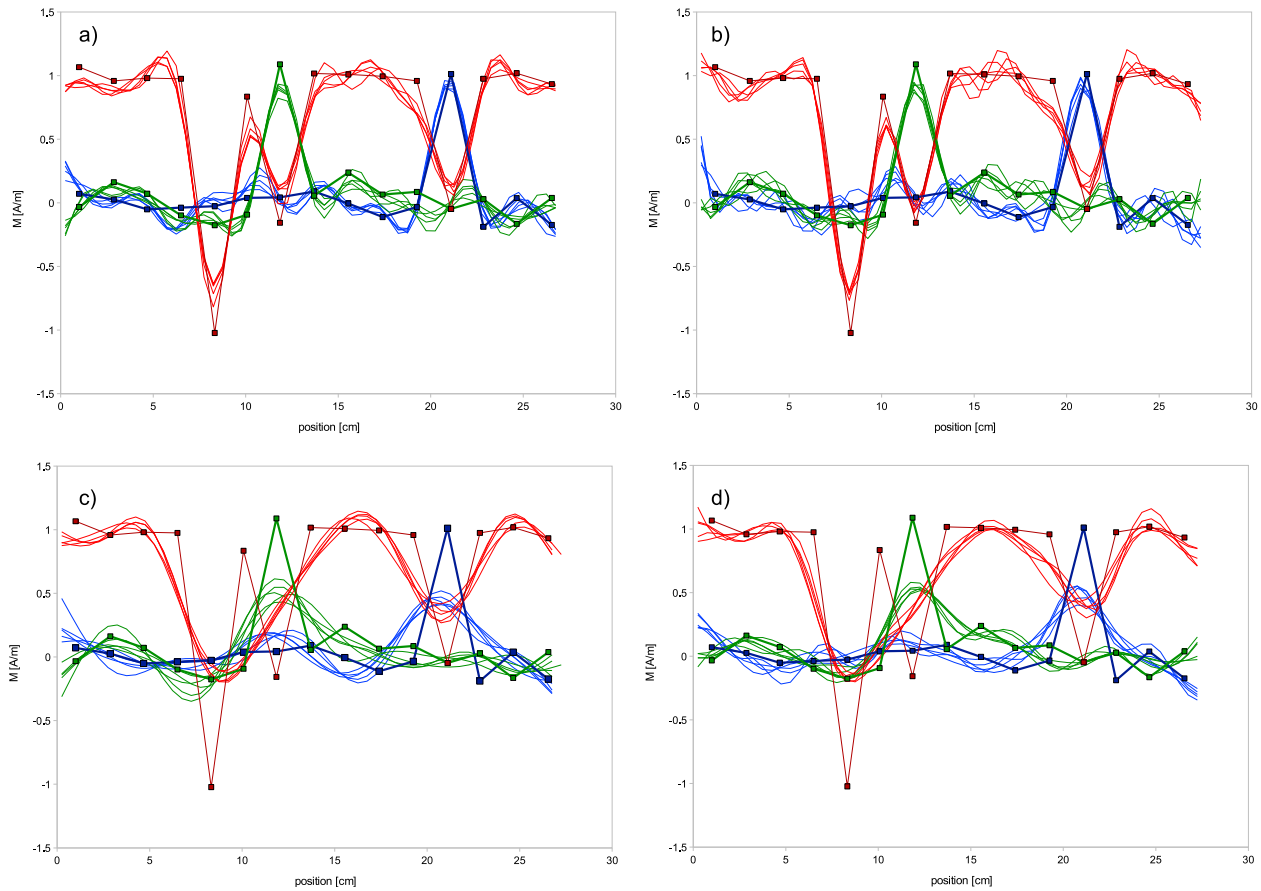
Figure 11. Artificial noise test. Red, green and blue respectively correspond to x, y and z components of magnetization. Five simulated data sets generated by adding Gaussian noise (standard deviation of 5×10^{-8} Am^2) to measured data before deconvolution with (a) ABIC minimization and (b) optimized RLS. Five simulated data sets generated by adding Gaussian noise (standard deviation of 5×10^{-7} Am^2) to measured data before deconvolution with (c) ABIC minimization and (d) optimized RLS. Discrete-sample measurements shown by squares for comparison.

channel are almost all within 2° of the z axis) but large variations in intensity (Figure 14). The small transverse (x and y) components of the measured vectors may be due to anisotropic acquisition of IRM or to the effects of tensor convolution. Deconvolution brings out intensity variations with larger amplitudes and finer length scales (Figure 14, z component), and also accentuates the directional variability: model transverse magnetic components (Figure 14, x and y components) commonly exceed 10% of the axial component (i.e., directions deviate by >5° from the z axis). Measurements on discrete cubes cut contiguously from the u channel show z-component variations in quite good agreement with those computed by deconvolution of the continuous-core measurements (Figure 14). There is little or no systematic difference between the results of ABIC minimization, SVD and RLS inversion.

[32] The x- and y-component variations measured on the discrete samples are comparable in magnitude to those measured in the continuous scan, but differ in the details of their downcore distribution. The discrete-sample transverse-component variations are much smaller than those obtained by deconvolution of the continuous-core scan (Figure 14). The deconvolved transverse-component variations are similar for all models, despite the significant difference between the response-function cross terms in the ABIC code and the two alternatives (the ABIC-minimization program does not include z-y, y-z, x-y or y-x terms but uses the same x-z and z-x terms as our full-tensor response function). The spurious x-component variations are driven in the same way for all the inversions by the strong variations in M_z, whereas y-component variations are in two cases (RLS and SVD) due to imperfect
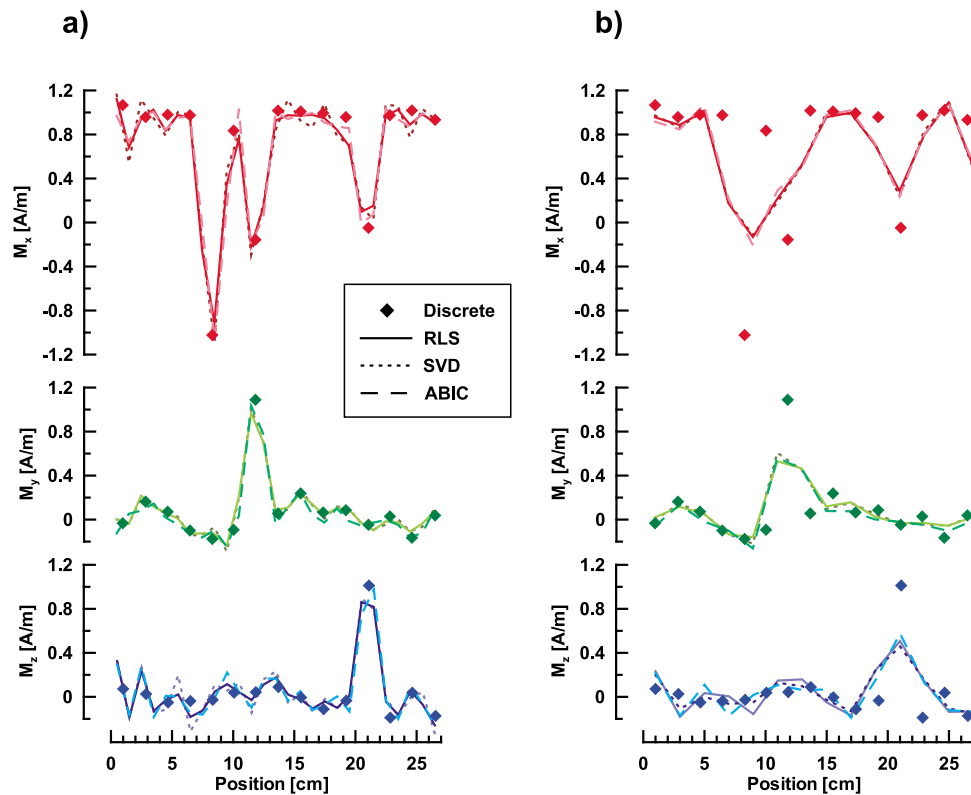
Figure 12. Sampling density test. Data set of experiment 3 (measured with 5-mm spacing) was resampled at (a) 10-mm spacing and (b) 20-mm spacing, and deconvolved using SVD, RLS and ABIC minimization. Discrete-sample measurements shown by diamonds for comparison. Red, green and blue respectively correspond to x, y and z components of magnetization.

calibration of R_{YZ} and in the remaining case (ABIC) due to entire omission of R_{YZ}.

6. Discussion

[33] Our major goal in this study has been to evaluate by direct experimentation the effects of varying several important aspects of the current state-of-the-art approach to deconvolution of continuous-core paleomagnetic data. In particular, we were interested in alternatives to explicit second-difference penalties, in the consequences of non-uniform measurement-error variance downcore, in the effects of over/undersampling, and in how these factors may interact.

[34] Second-difference minimization, as stated above, is a very logical approach to constrained inversion, because second differences represent linear combinations of model parameters that are poorly constrained by the data. Nevertheless, it is conceivable that in some circumstances alternative constraints might produce better models. Our experiments involving downcore directional changes

with essentially invariant intensity were designed to explore this. Accurate $\vec{M}(z)$ models are required to have almost exactly the same total size (L2 norm) in all three of these experiments, but significantly different summed squared second differences, increasing as the number and magnitude of directional shifts increases. For experiments 2 and especially 3, accurate models are required to have large second differences, particularly when the sampling interval and spacing of model elements approach the length scale of real magnetic variations. For the lake sediment IRM, penalizing total model size might be expected to suppress downcore intensity variations in the optimized SVD and RLS models. In view of these considerations it seemed plausible that algorithms with different penalty functions (second differences and total model size) would produce different optimized models over the series of experiments. It is interesting that this turned out not to be the case: the three techniques in each of our experiments converge to essentially the same solutions. On the one hand this is not too surprising, since the techniques all solve essentially the same matrix equation (same
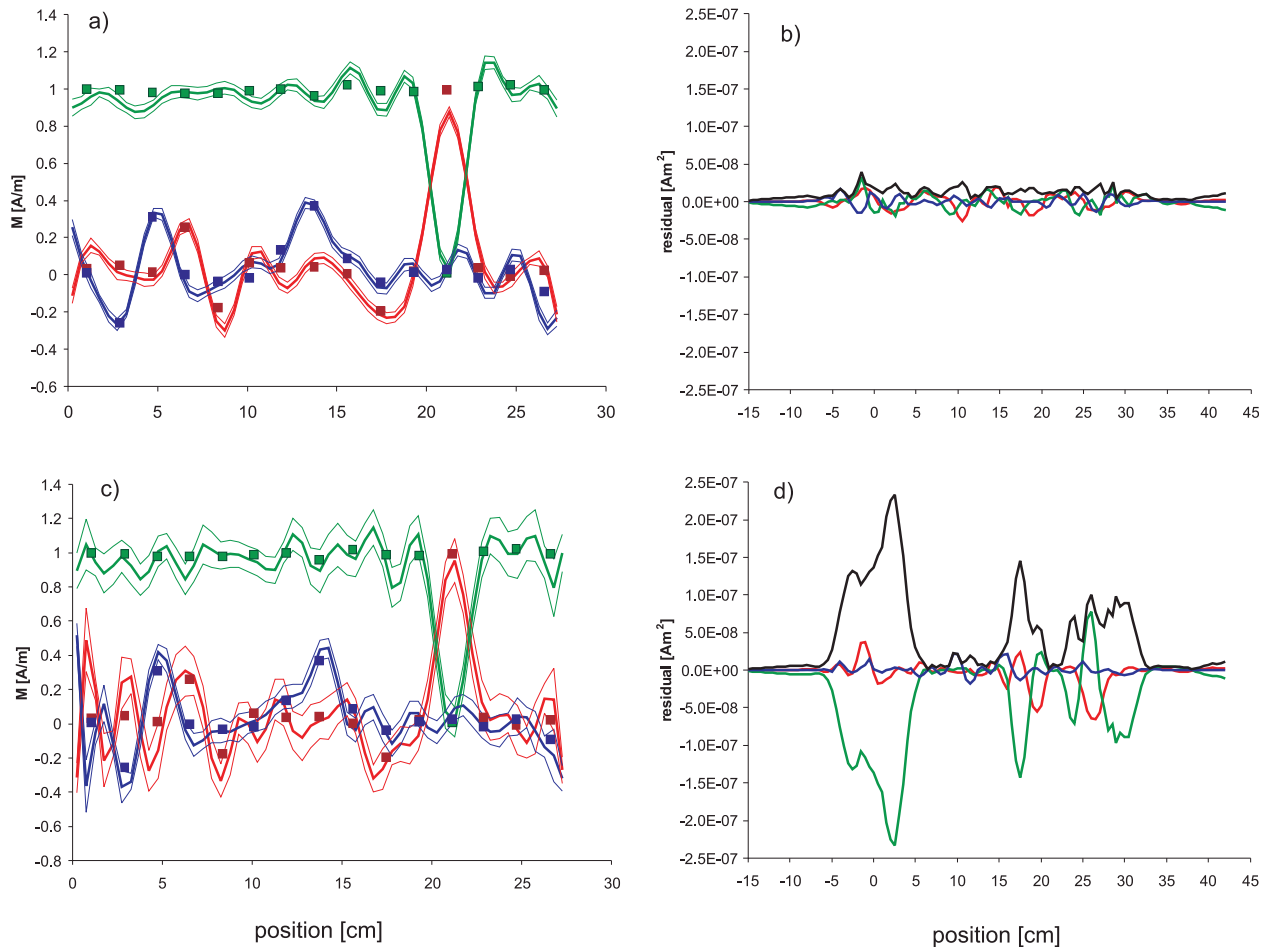
Figure 13. Effect of position-dependent measurement errors. Red, green and blue correspond to x, y and z vector components. (a) Model with position-independent $\sigma_D = 1 \times 10^{-8}$ Am^2, with 95% confidence intervals and discrete-sample measurements shown by squares for comparison. (b) Residuals of the model in Figure 13a; black shows total vector length $(D_x^2 + D_y^2 + D_z^2)^{1/2}$. RMS misfit is 1.3×10^{-8} Am^2. (c) Model with position-dependent $\sigma_D = 2 \times 10^{-10}$ Am^2 + dD/dz*0.02cm, with 95% confidence intervals and discrete-sample measurements shown by squares for comparison. (d) Residuals of the model in Figure 13c; black shows total vector length. RMS misfit is 7.0×10^{-8} Am^2.

response function and same data set), and it is only the stabilizing mechanisms and evaluation criteria that differ. Moreover in SVD the functions eliminated from the basis set by zeroing small singular values are generally those with large second differences, so even though the zeroing criteria are based on total model size and residual, the effect is understandably quite similar to that of explicit second-difference minimization. Nevertheless it is significant that the three algorithms always converge so closely in the relatively large space of potentially acceptable solution vectors, given the large changes in the relative magnitudes of the different penalty functions over the set of experiments. In practice this result provides assurance that the solutions obtained by any one of these approaches are indeed optimal.

[35] When measurement errors are assumed to be normally distributed with position-independent variance, as assumed in the ABIC code, the measured data are all given equal weight in calculating an optimally fit magnetization model. This assumption is not generally warranted, but our results show that even when it is grossly in error, it still appears to be useful, improving the stability and accuracy of the inverse modeling. When we incorporate a more realistic model of data errors with depth-dependent variance, measurements from high-gradient sections of a core are given much less weight, due to the direct translation of small position uncertainties into relatively large magnetic measurement uncertainties. Despite our hope that properly accounting for this error distribution in the inverse calculations would improve the outcome, the reverse is true.
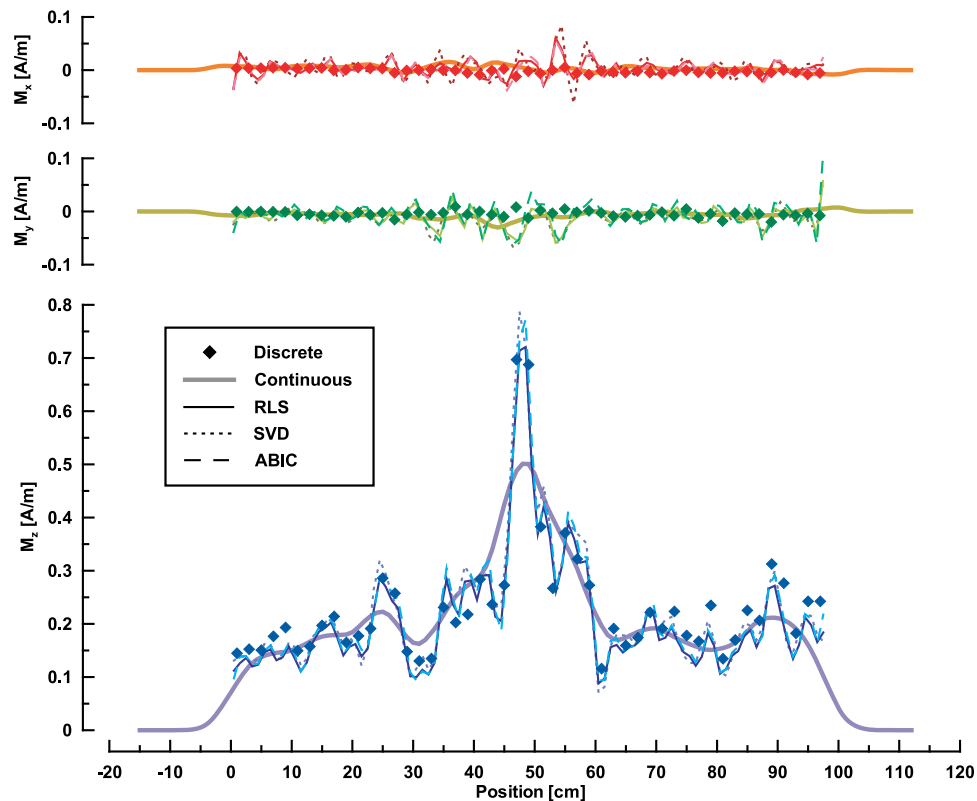
Figure 14. Pulsed-field (along z axis) IRM of the Deming Lake sediment u channel. Bold curves show continuous-scan measured moments normalized by effective volume (u channel cross-sectional area times effective sensed length [e.g., *Roberts*, 2006]). Finer curves show magnetization models obtained by deconvolution of the continuous measurements using SVD, RLS, and ABIC-minimization. Measurements on discrete cubes after subsampling (diamonds) generally agree well with the deconvolved models.

Discounting the measurements in high-gradient regions reduces stability and accuracy because these are the measurements that most directly indicate significant downcore changes in magnetization. Improvement in the accuracy of sample positioning would be extremely beneficial but in practice is very difficult to achieve. We tested a commercial laser-positioning system (Acuity AR1000) mounted in line with the u channel track, but found that its accuracy and reproducibility (a few hundred microns) were not adequate to resolve the variability in positions set by stepper-motor counts. Replacement of the stepper motor by a servo motor and controller in the Bremen lab instrument resulted in significant improvement (K. Fabian, personal communication, 2009). However, even if positioning errors can be reduced to a standard deviation of tens of microns, they will still often produce measurement errors that are large compared to high-frequency instrument noise, and the effective signal/noise ratio of the system will be self-limiting near u channel ends and near sharp internal changes in magnetization orientation/intensity.

[36] An ultimate limitation on resolution of down-core magnetization changes is the width of the instrument response function. *Oda and Shibuya* [1996] found that for the magnetometer then on the *Joides Resolution*, with a response-function width (at half height) of ~11cm, they could accurately deconvolve to a resolution of ~2 cm in favorable cases. For 2G systems with "high-resolution" coil geometry, the response function width is about 5 cm [*Guyodo et al.*, 2002], and proportional resolution would be ~1 cm, assuming high s/n ratios and low damping parameters (u, ζ or α). *Guyodo et al.* [2002] tested this by sub-sampling two u channels in contiguous 1-cm lengths, and found that the discrete-sample measurements exhibited much stronger variations in direction and intensity than were seen in the deconvolved whole-core data. They suggested that the differences could be attributed either to inaccuracies in the deconvolution calculations (due for

example to omission of some cross terms from the response function) or to real differences in the magnetization of the subsamples (due for example to sediment disturbance or positioning errors during cutting). To this list we would add the fact that a narrower response function necessarily produces stronger signal gradients at the core ends and near locations within the core where magnetization intensity or direction change sharply, and therefore positioning errors are translated into larger errors in the measured signal. In this way, somewhat paradoxically, the narrower response function may hinder resolution in some ways while helping in others.

[37] *Oda and Shibuya* [1996] evaluated the importance of the response-function cross terms by deconvolving a data set using different response functions that included or omitted cross terms, and concluded that the differences were generally not of major significance. Our results for the sediment core with an axial IRM confirm this. Erroneously large transverse components in the deconvolved model magnetizations must result from imperfect calibration of the response-function cross terms R_{XZ} and R_{YZ}. Omission of the latter term in the ABIC-minimization code results in erroneous y components comparable to those calculated by RLS and SVD using the full response tensor. In principle these should be correctable by using a more accurate response function. In practice however it would appear that other sources of error generally are more important, as concluded by *Oda and Shibuya* [1996]. It is also interesting to note that the optimal damping level differs for the three directional-component magnetizations according to their relative intensities: the x- and y-component models are clearly underdamped, given the lower signal/noise ratios in the x- and y-component data. For this reason, separate inversions for the individual directional components (as in the work by *Constable and Parker* [1991]) may in some cases be preferable to simultaneous solution for the three vector components of $\vec{M}(z)$ using the tensor response and full data vectors.

7. Summary and Conclusions

[38] In previous approaches to deconvolution of continuous-core paleomagneic data, high-frequency noise has been assumed to be the dominant source of measurement error. In other words, it is assumed that random signal fluctuations occur primarily on timescales sufficiently short that the measurement-error probability distribution for each position in a scan is unrelated to the error in neighboring positions. Our results, based on extended noise measurements and on replicate scans of several u channels, show that this assumption is commonly unwarranted. The noise spectrum includes significant power in periodicities comparable to the time required to scan a core (~5 to 30 min); these variations are not removed by linear drift correction, nor do the errors average to zero over substantial core intervals. Such errors can only be detected and characterized by performing replicate scans (as in, e.g., the work by *Guyodo et al.* [2002]). Moreover irreproducibility and inaccuracy in sample positioning are major sources of measurement error, especially in portions of a core where there are large gradients in the measured signal. Somewhat paradoxically, when we incorporate a more accurate model of measurement errors into the inverse calculations, the deconvolved magnetization distributions are less accurate and have more spurious variation. Discounting the measurements in high-gradient regions reduces stability and accuracy because these are the measurements that most directly reflect significant changes in core magnetization.

[39] In general, the different optimization techniques that we have evaluated (RLS, SVD and ABIC) all produce dramatically improved estimates of the true magnetization distribution when (a) the signal/noise ratio exceeds a few hundred, (b) the sampling interval is no more than half the lengthscale of magnetization changes downcore, and (c) the response function is accurately specified. Moreover for all three methods, the magnetization models are degraded in the same way, and at the same rate, when any of these three conditions is not fully realized. Future improvements will require more effective ways to deal with positioning errors, both in terms of statistical methods for addressing the resulting measurement uncertainties, and in terms of technical improvements in setting and measuring positions accurately.

Acknowledgments

References

Clarke, J. (1993), SQUIDs: Theory and practice, in *The New Superconducting Electronics*, edited by H. Weinstock and R. W. Ralston, pp. 123–180, Kluwer Acad., Dordrecht, Netherlands.

Constable, C., and R. Parker (1991), Deconvolution of long-core palaeomagnetic measurements—Spline therapy for the linear problem, *Geophys. J. Int.*, *104*, 453–468, doi:10.1111/j.1365-246X.1991.tb05693.x.

Dodson, R. E., M. D. Fuller, and W. Pilant (1974), On the measurement of the remanent magnetism of long cores, *Geophys. Res. Lett.*, *1*, 185–188, doi:10.1029/GL001i004p00185.

Guyodo, Y., J. E. T. Channell, and R. G. Thomas (2002), Deconvolution of u-channel paleomagnetic data near geomagnetic reversals and short events, *Geophys. Res. Lett.*, *29*(17), 1845, doi:10.1029/2002GL014927.

Hansen, P. C. (1998), *Rank-Deficient and Discrete Ill-Posed Problems: Numerical Aspects of Linear Inversion*, Soc. for Ind. and Appl. Math., Philadelphia, Pa.

Liu, Q. S., A. P. Roberts, E. J. Rohling, R. X. Zhu, and Y. B. Sun (2008), Post-depositional remanent magnetization lock-in and the location of the Matuyama-Brunhes geomagnetic reversal boundary in marine and Chinese loess sequences, *Earth Planet. Sci. Lett.*, *275*(1–2), 102–110, doi:10.1016/j.epsl.2008.08.004.

Oda, H., and H. Shibuya (1994), Deconvolution of whole-core magnetic remanence data by ABIC minimization, *J. Geomagn. Geoelectr.*, *46*, 613–628.

Oda, H., and H. Shibuya (1996), Deconvolution of long-core paleomagnetic data of Ocean Drilling Program by Akaike's Bayesian Information Criterion minimization, *J. Geophys. Res.*, *101*, 2815–2834, doi:10.1029/95JB02811.

Parker, R. L., and J. S. Gee (2002), Calibration of the pass-through magnetometer. II. Application, *Geophys. J. Int.*, *150*(1), 140–152, doi:10.1046/j.1365-246X.2002.01692.x.

Press, W. H., B. P. Flannery, S. Teukolsky, and W. T. Vetterling (1986), *Numerical Recipes: The Art of Scientific Computing*, 814 pp., Cambridge Univ. Press, Cambridge, U. K.

Roberts, A. P. (2006), High-resolution magnetic analysis of sediment cores: Strengths, limitations and strategies for maximizing the value of long-core magnetic data, *Phys. Earth Planet. Inter.*, *156*(3–4), 162–178, doi:10.1016/j.pepi.2005.03.021.

Roberts, A. P., and M. Winklhofer (2004), Why are geomagnetic excursions not always recorded in sediments? Constraints from postdepositional remanent magnetization lock-in modelling, *Earth Planet. Sci. Lett.*, *227*, 345–359, doi:10.1016/j.epsl.2004.07.040.

Sagnotti, L., P. Rochette, M. Jackson, F. Vadeboin, J. Dinares-Turell, and A. Winkler (2003), Inter-laboratory calibration of low-field magnetic and anhysteretic susceptibility measurements, *Phys. Earth Planet. Inter.*, *138*(1), 25–38.

Schneider, D. A., D. V. Kent, and G. A. Mello (1992), A detailed chronology of the Australasian impact event, the Brunhes-Matuyama geomagnetic polarity reversal, and global climate change, *Earth Planet. Sci. Lett.*, *111*, 395–405.

Shcherbakov, V., and N. Sycheva (2010), On the mechanism of formation of depositional remanent magnetization, *Geochem. Geophys. Geosyst.*, *11*, Q02Z13, doi:10.1029/2009GC002830.

Shibuya, H., and T. Michikawa (2000), Calculation of superconducting rock magnetometer response, *Kumamoto J. Sci. Earth Sci.*, *16*(2), 1–16.

Tauxe, L., J. L. LaBrecque, R. Dodson, M. Fuller, and J. DeMatteo (1983), "U" channels: A new technique for paleomagnetic analysis of hydraulic piston cores, *Eos Trans. AGU*, *64*(18), 219.

Teanby, N., and D. Gubbins (2000), The effects of aliasing and lock-in processes on palaeosecular variation records from sediments, *Geophys. J. Int.*, *142*(2), 563–570, doi:10.1046/j.1365-246x.2000.00180.x.

Weeks, R., C. Laj, L. Endignoux, M. Fuller, A. Roberts, R. Manganne, E. Blanchard, and W. Goree (1993), Improvements in long-core measurement techniques: Applications in palaeomagnetism and palaeoceanography, *Geophys. J. Int.*, *114*, 651–662.

Zięba, A. (1993), Image and sample geometry effects in SQUID magnetometers, *Rev. Sci. Instrum.*, *64*(12), 3357–3375, doi:10.1063/1.1144306.